ROBUST ELECTROSTATIC INCHWORM MOTORS FOR MACROSCOPIC MANIPULATION AND MOVEMENT

Daniel Teal[1], Hani C. Gomez[1], Craig B. Schindler[1], and Kristofer S. J. Pister[1]
[1]UC Berkeley, Berkeley, USA

2021 21st International Conference on Solid-State Sensors, Actuators and Microsystems (Transducers) | 978-1-6654-1267-4/21/$31.00 ©2021 IEEE | DOI: 10.1109/TRANSDUCERS50396.2021.9495446

ABSTRACT

We report robust microfabricated MEMS electrostatic inchworm motors moving macroscopic objects: a motor in a 14.5x9.5x1.2mm gripper with 3mm displacement and 15mN force lifting a 1g weight, and an identical motor moving a 100mm long 230mg shuttle an 80mm distance horizontally at up to 5mm/s. This is an order of magnitude larger than previous electrostatic inchworm motors and demonstrates competitiveness with piezoelectric motors for millimeter-scale actuation for microrobotics.

KEYWORDS

electrostatic inchworm motor, microrobot, microgripper

INTRODUCTION

Millimeter-scale microrobotics makes use of a variety of actuation technologies: electrostatics, piezoelectrics, shape memory alloys, and external magnetic fields, among others, and microrobot design is currently limited by the ability to integrate these actuators into complete systems [1]. While piezoelectric actuators currently span the widest range of performance characteristics [2] and have been used in impressive autonomous microrobots [3], electrostatic inchworm motors potentially offer similarly good performance but can also be more easily microfabricated and miniaturized—for example, a motor can be created in a single-mask SOI process [4].

In this work, we reinforce a previously published electrostatic inchworm motor [5] then use it to perform larger millimeter-scale microrobotic tasks than originally reported. First, we integrate the motor into a microgripper capable of lifting a 1g weight (Fig. 1a), a 5x increase from the original work. This can also be compared favorably to piezoelectric grippers [6] and the general literature [7]. Second, we demonstrate the same motor moving 80mm (Fig. 1b), illustrating the capacity of electrostatic inchworm motors to move arbitrarily long distances [4]. This 80mm movement is over an order of magnitude further than that of any other electrostatic inchworm motor to date.

We believe these results illustrate that electrostatic inchworm motors scale to sizes and performances relevant to larger microrobots and can compete with piezoelectric actuators to do so.

MOTOR IMPLEMENTATION

Motor Architecture

We begin with the same electrostatic inchworm motor design used in [5], which is an implementation of the motor architecture proposed in [4] and studied in [8]. Fig. 2 reviews its basic operation and some parameters that may be of interest to the reader. We then reinforce the motor to integrate it into a gripper and with a long shuttle.

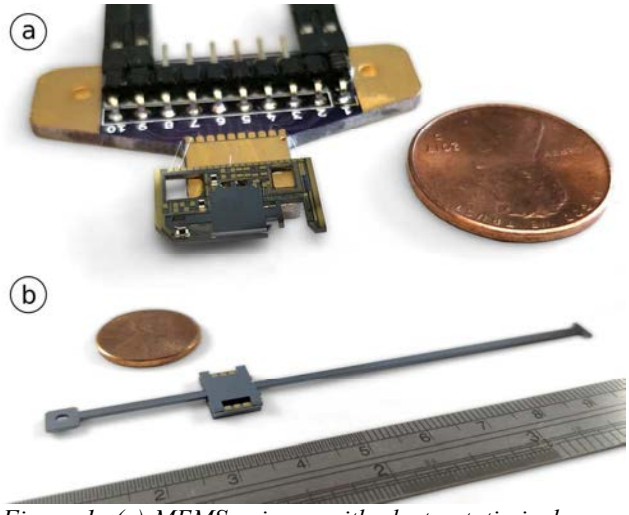

Figure 1: (a) MEMS gripper with electrostatic inchworm motor mounted to a PCB with 19mm diameter US penny for scale. (b) Motor with a 100mm long shuttle.

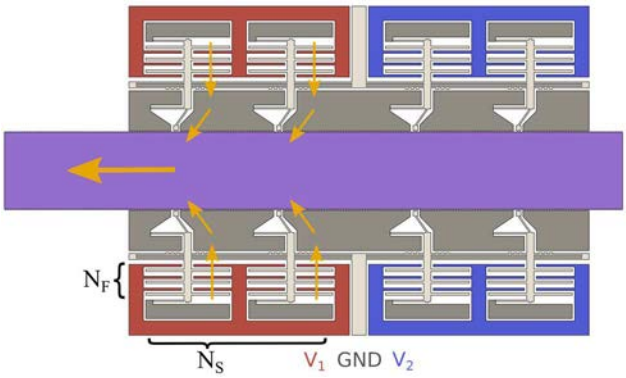

Figure 2: A simplified diagram of the electrostatic inchworm motor architecture of [1] and implemented in [5] and here. On the device layer of an SOI process are manufactured two actuator arrays (here, red and blue). When an array is energized, a large number $2 \cdot N_F \cdot N_S$ of gap-closing actuator fingers (with N_F finger pairs on each of N_S spines; in this figure, $N_F = 6$, $N_s = 2$) move spines (white) toward a shuttle (purple). Angled driving arms on the spines cause the shuttle to move laterally a small amount (orange arrows). Progressively engaging the two arrays 180 degrees out of phase results in shuttle movement. For the motor in this work, $N_F = 96$, $N_S = 8$, for a total of $4 \cdot N_F \cdot N_S = 3072$ finger pairs. Note the shuttle has bumps along its side (here, with 4µm pitch) that the angled driving arms engage with; this defines the length of each step. We currently drive the motors with 75% duty cycle square voltage waves; changing the frequency adjusts the speed of the motor.

Mechanical Reinforcement

Our first modification is to significantly strengthen the motor shuttle. In [4] and [5], the shuttle is fabricated solely from the SOI device layer with the rest of the motor.

However, when the shuttle extends beyond the motor edge as required for many applications, it may be subject to significant external forces. Treating the shuttle as a simple beam with one end fixed at the motor and an external force on the end estimates its maximum stress:

$$\sigma_{max} \approx \frac{6 \cdot F \cdot L}{b \cdot h^2}$$

Without modification, our motor, with a shuttle h=40µm thick, b=1mm wide, and extended L=10mm, would break with a low ≈40mN force applied assuming 1.6GPa silicon tensile strength. Instead, as shown in Fig. 3B, we strengthen the shuttle with a 550µm-thick substrate-layer beam, manufactured in the same through-substrate DRIE etch used to define the motor edges and singulate devices, to withstand >1N applied out-of-plane force.

Simultaneously, in order to prevent the shuttle from moving up out of plane, we bond a cover on top of the motor using silver epoxy (shown in Fig. 3a) with the convenient side effect of protecting the motor from dust. We use epoxy as standard chip bonders cannot easily hold the parts given the DRIE substrate etch (nor are chip bonders scalable to arbitrary microrobot shapes).

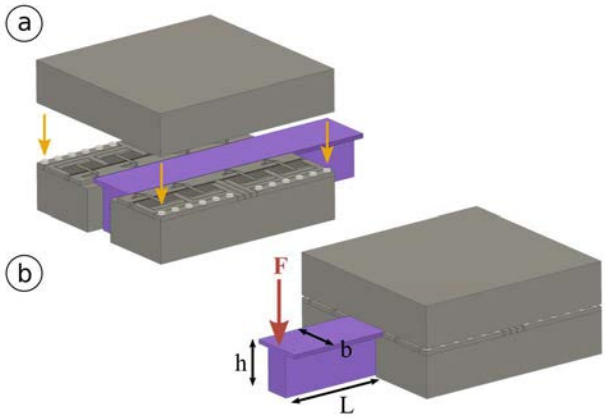

Figure 3: Simplified illustrations of the reinforcement. (a) The motor shuttle (purple) is T-shaped, using the substrate layer for strength, and a cover is bonded on top with dots of silver epoxy. (b) Beam deflection theory approximates the maximum out-of-plane force the shuttle can withstand.

Contamination Resistance

Approximately 50% of our devices have at least one particle (5 to 50µm) deposited on the motor during fabrication and assembly that mechanically prevents the motor fingers from closing. To increase yield, we make all connections between spines sufficiently compliant that the motor will operate around a single stuck spine, albeit at a reduced capacity as shown in Fig. 4. With a particle, the motor force decreases to:

$$F_{with\ particle} = F_0 \cdot \frac{N_S - 1}{N_S}$$

So N_S (defined in Fig. 2) should be high to retain capacity (here, $N_S = 8$). This resilience, combined with the motor cover to reduce dust incidence, may also aid operation in non-cleanroom environments.

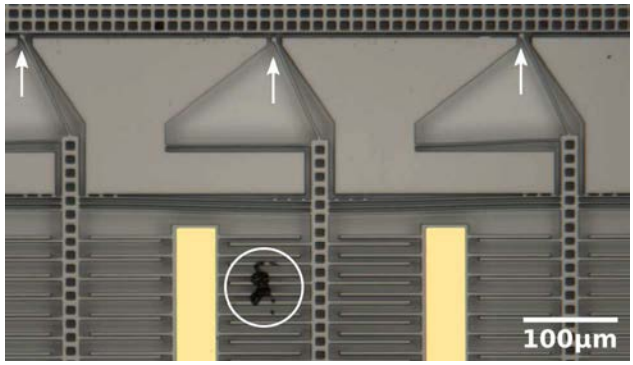

Figure 4: A micrograph of motor fingers and spines as fabricated and engaged with the shuttle. A black particle, circled, prevents the spine in the center from moving. However, the spines on either side move independently and do engage, demonstrating contamination resistance.

Fabrication

We fabricate these motors and devices in the same three-mask 40-2-500µm SOI process used in [5], but after the device backside singulation etch, the motor cover chip is bonded on top with epoxy. Fig. 5 details the process.

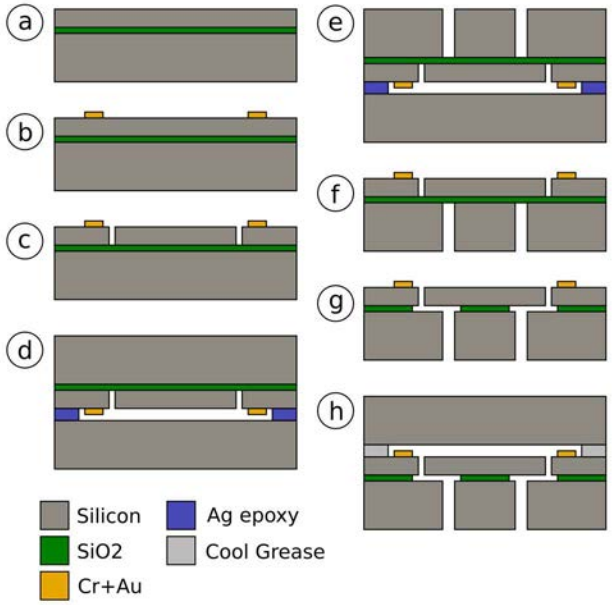

Figure 5: Fabrication process. (a) 40-2-550µm SOI wafer, 20ohm-cm p-doped, <100>, (b) liftoff pattern 500nm Cr + Au for external electrical contacts, (c) DRIE etch 40um device layer, (d) temporarily bond frontside to handle wafer with Cool Grease (not placed on MEMS fingers), (e) DRIE etch through backside to singulate devices and define shuttle substrate, (f) remove devices from wafer with tweezers, (g) timed HF vapor oxide release etch, (h) stamp silver epoxy (EC 151-L from Polytec PT distributed by all4-GP North America Inc.) on top and add cover (fabricated in the same process).

EXPERIMENTAL RESULTS

MEMS Gripper

To demonstrate a purely microrobotic application and compare directly to [5] and [6], we constructed a MEMS gripper as shown in Fig. 1(a). A 1mm wide shuttle moves

up to 3mm to hold an object and is retracted by a spring when the motor is released. Fig. 6 shows the gripper layout with integrated motor, and Fig. 7 shows the gripper successfully lifting assorted objects up to 1.2g.

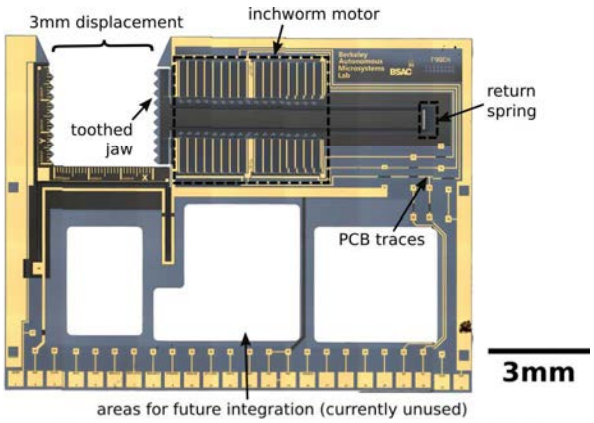

Figure 6: Stitched micrograph of (a version of) the gripper before cover is attached. The motor, shuttle, and retraction spring are visible near the top. Silicon PCB traces connect the sides of the inchworm and can be used for future circuitry integration. The gold layer reduces resistance to external contacts and within the traces.

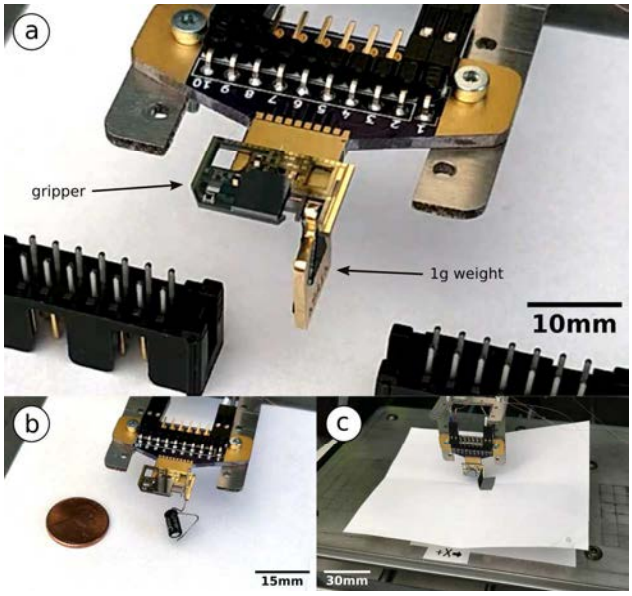

Figure 7: The gripper lifting (a) a 1.0g brass weight, (b) a 0.2g capacitor as in [3], (c) a 1.2g folded piece of paper.

Long Shuttle Motor

To demonstrate arbitrarily long displacements, we created a motor with a 100mm long shuttle (80mm stroke) as shown in Fig. 1(b). The shuttle is patterned with a Heidelberg MLA150 maskless aligner so that the only limit to its length is the diameter of the SOI wafer used (here, 150mm). The inchworm motor halves are held in place around the shuttle by epoxied stacked top and bottom chips. The halves must remain aligned to each other within about 2µm in order for the angled driving arms to engage the shuttle correctly, so we fabricate them with a sacrificial silicon jig to maintain position during stack assembly. We show the microfabricated components in Fig. 8, the assembly process in Fig. 9, and testing results in Fig. 10.

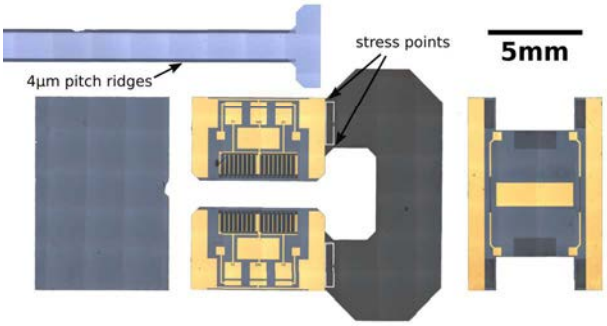

Figure 8: Stitched micrographs of the long shuttle motor components to be stacked. Top, the shuttle. Left: the stack bottom, a silicon rectangle. Center: two inchworm motor halves, held together within 2µm precision by a sacrificial jig connected at stress-concentrating points designed to break with ≈10N of force. Right: the top cover chip.

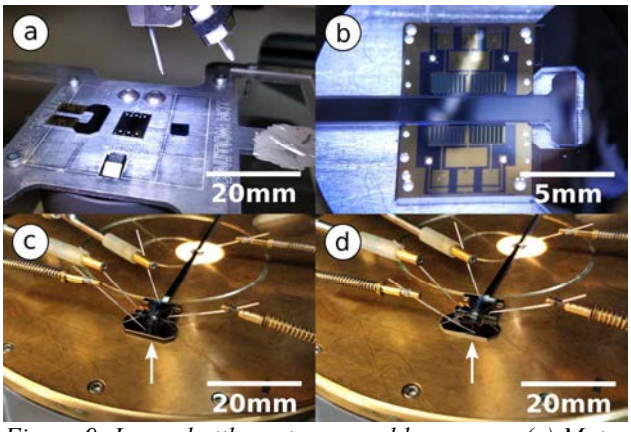

Figure 9: Long shuttle motor assembly process. (a) Motor bottom and center on die bonder tool used to stamp epoxy and align parts. (b) Close-up of epoxy stamped on motor with the shuttle in place. (c) After stack is complete and epoxy is cured, a probe applies about 1 to 10N of force on the sacrificial jig. (d) The jig is pushed down and broken off motor. Motor is then complete as shown in Figs. 1, 10.

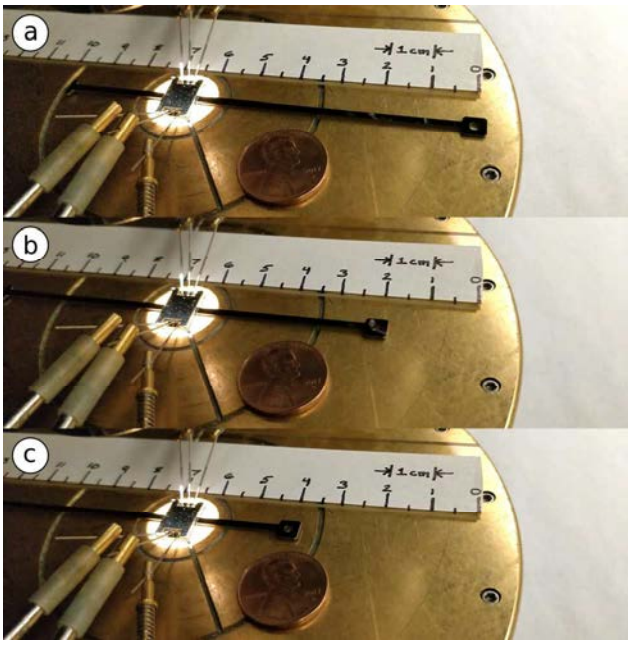

Figure 10: The long shuttle motor on a probe station moving at 5mm/s at times (a) t=0s, (b) t=4s, (c) t=8s.

DISCUSSION

We list relevant parameters of the gripper and long shuttle motor in Table 1 for comparison with other actuators. We recommend referencing Table 1 of [4] for inchworm motors, Table 1 of [6] for piezoelectric grippers, or Fig. 1 of [2] or [7] for generic actuators.

Table 1: Summary of tested system parameters. Note the motor structures are identical to each other and [3] so they share certain parameters (motor size, force). The motor size refers to the bounding box of the gap-closing actuator arrays on the SOI device layer. The tested speed, efficiency, and power are for 100V, 1mm/s, no load conditions. The power measurements are approximate to a factor of 10. The efficiency is approximated by force times speed over measured power. The shuttle has been experimentally run at higher speeds (up to 5mm/s) than the gripper. Above the given speeds, these devices occasionally stall for undetermined reasons we suspect are friction-related.

Parameter	Gripper	Long Shuttle
Total Size (mm)	14.5x9.5x1.2	100x11.5x1.8
Motor Size (mm)	4.7x3x0.04	4.7x3x0.04
Total Mass (mg)	180	590
Shuttle Mass (mg)	13	230
Capacity (g)	> 1.2	n/a
Stroke (mm)	3	80
100V Force (mN)	15	15
Max Speed (mm/s)	1	5
Power (mW)	1	1
Efficiency (%)	2	2

In particular, [5], which describes the motor we modify, reports a gripper holding 0.2g, 5x less than demonstrated here. The piezoelectric gripper described in [6], comparable to others, reports a 268µm stroke with 575mN in a 0.1g actuator. Our gripper of similar mass can displace significantly longer distances but with less than one-tenth the force. However, the mass of just the gap-closing actuators in our motor is approximately 10mg, improving force/mass density.

To the best of the authors' knowledge, the furthest published electrostatic inchworm movement is 3mm [5], and [9] compares qualitatively different inchworms with a maximum 5mm displacement. [2], which compares displacements of multiple types of actuators, appears out of date but reports 100µm movement. All of these values are at least one order of magnitude below the 80mm stroke demonstrated in this work. At this point, displacement length is limited merely by microfabrication equipment.

We believe these results illustrate that electrostatic inchworm motors scale to sizes and performances relevant to larger microrobots and can compete with piezoelectric actuators to do so, and hope this results in more routes toward microrobotic system integration in the future.

ACKNOWLEDGEMENTS

Thanks to Dillon Acker-James for help and discussion and to the Berkeley Sensor & Actuator Center for administrative support. Devices were fabricated in the UC Berkeley Marvell Nanofabrication Laboratory. This material is based upon work supported by the National Science Foundation Graduate Research Fellowship Program under Grant No. DGE 1752814.

REFERENCES

[1] R. St. Pierre and S. Bergbreiter, "Toward Autonomy in Sub-Gram Terrestrial Robots," *Annual Review of Control, Robotics, and Autonomous Systems*, vol. 2, no. 1, pp. 231–252, 2019, doi: 10.1146/annurev-control-053018-023814.

[2] D. J. Bell, T. J. Lu, N. A. Fleck, and S. M. Spearing, "MEMS actuators and sensors: observations on their performance and selection for purpose," *J. Micromech. Microeng.*, vol. 15, no. 7, pp. S153–S164, Jun. 2005, doi: 10.1088/0960-1317/15/7/022.

[3] K. Jayaram, J. Shum, S. Castellanos, E. F. Helbling, and R. J. Wood, "Scaling down an insect-size microrobot, HAMR-VI into HAMR-Jr," in *2020 IEEE International Conference on Robotics and Automation (ICRA)*, May 2020, pp. 10305–10311, doi: 10.1109/ICRA40945.2020.9197436.

[4] I. Penskiy and S. Bergbreiter, "Optimized electrostatic inchworm motors using a flexible driving arm," *J. Micromech. Microeng.*, vol. 23, no. 1, p. 015018, Dec. 2012, doi: 10.1088/0960-1317/23/1/015018.

[5] C. B. Schindler, H. C. Gomez, D. Acker-James, D. Teal, W. Li, and K. S. J. Pister, "15 Millinewton Force, 1 Millimeter Displacement, Low-Power MEMS Gripper," in *2020 IEEE 33rd International Conference on Micro Electro Mechanical Systems (MEMS)*, Jan. 2020, pp. 485–488, doi: 10.1109/MEMS46641.2020.9056128.

[6] T. Abondance, K. Jayaram, N. T. Jafferis, J. Shum, and R. J. Wood, "Piezoelectric Grippers for Mobile Micromanipulation," *IEEE Robotics and Automation Letters*, vol. 5, no. 3, pp. 4407–4414, Jul. 2020, doi: 10.1109/LRA.2020.2997317.

[7] A. Dochshanov, M. Verotti, and N. P. Belfiore, "A Comprehensive Survey on Microgrippers Design: Operational Strategy," *Journal of Mechanical Design*, vol. 139, no. 070801, May 2017, doi: 10.1115/1.4036352.

[8] D. S. Contreras and K. S. J. Pister, "Dynamics of electrostatic inchworm motors for silicon microrobots," in *2017 International Conference on Manipulation, Automation and Robotics at Small Scales (MARSS)*, Jul. 2017, pp. 1–6, doi: 10.1109/MARSS.2017.8001936.

[9] M. A. Erismis, H. P. Neves, R. Puers, and C. V. Hoof, "A Low-Voltage Large-Displacement Large-Force Inchworm Actuator," *Journal of Microelectromechanical Systems*, vol. 17, no. 6, pp. 1294–1301, Dec. 2008, doi: 10.1109/JMEMS.2008.2004852.

CONTACT

*Daniel Teal, dteal@berkeley.edu